Journal of Nanoscience and Technology 2(2) (2016) 122–125

ISSN: 2455-0191

Contents List available at JACS Directory

Journal of Nanoscience and Technology

journal homepage: www.jacsdirectory.com/jnst

The Effect of Inter-Protofilament Sliding on the Mechanics of Microtubules

Zhigang Guo, Chengyuan Wang*

School of Civil Engineering and Mechanics, Jiangsu University, No 301 Xuefu Road, Zhenjiang, Jiangsu – 212013, China.

ARTICLE DETAILS

Article history:
Received 15 May 2016
Accepted 25 May 2016
Available online 30 May 2016

Keywords:
Microtubules in Cells
Inter-Protofilament Sliding
Transverse Vibration

ABSTRACT

Inter-Protofilament (*PF*) sliding has been observed experimentally for microtubules (MTs) in eukaryotic cells. This paper aims to quantitatively examine its effect on the static bending and transverse vibration of MTs. In calculating the bending stiffness and the frequencies a newly developed molecular structural mechanics (MSM) technique able to capture the relative sliding between the adjacent *PF*s was compared with the Euler beam model where the inter-*PF* sliding is neglected. The difference between the two models thus measures the effect of the inter-*PF* sliding on the mechanics of MTs. Significant effect of the inter-*PF* sliding is achieved in the present study, leading to lower bending stiffness and the downshift of the frequency of MT vibration. In particular, the effect of the inter-*PF* sliding is found to increase with decreasing deformation wavelength-to-diameter ratio.

1. Introduction

Microtubules (MTs) found in eukaryotic cells play an important role in maintaining cell shape and structural stiffness, providing tracks for intracellular transport and facilitating cell division and motility [1]. These nanotubes (diameter 25 nm) are protein polymer with a hollow cylindrical filamentous structure. In MTs, α and β tubulines [2] are connected head to tail to construct the protofilaments (*PF*s) bonded laterally via inter-*PF* bonds (i.e., $\alpha\alpha$ and $\beta\beta$ bonds between two adjacent *PF*s) to form the cylindrical lateral surface of MTs (Fig. 1). It is found that the intra-*PF* $\alpha\beta$ bonds are much stronger than the inter-*PF* $\alpha\alpha$ and $\beta\beta$ bonds.

In the last two decades a great deal of effort was made to explore the mechanical responses of MTs [3-16], where static deformation [4, 5, 9], structural instability [7, 14] and vibrations [6, 8, 16] are among the major issues of great interest. In particular, the inter-*PF* sliding (0.2 nm) was observed for the grafted MTs in the experiments [3, 4] which is considered as a result of the weak inter-*PF* interactions. It is believed that the occurrence of the inter-*PF* sliding makes the MTs more compliant when they are subjected to an external loadings, e.g., a force, a moment or a strain. This indeed necessitates a study to examine the effect of the inter-*PF* sliding on the mechanics of MTs. Nevertheless, the existing continuum mechanics models [6-8] are unable to account for the inter-*PF* sliding while the molecular dynamics simulations [12] are computationally expensive. Under this circumstance, up till now no detailed quantitative research has been reported on the aforementioned issue.

Recently, a molecular structural mechanics (MSM) model [14-16] has been developed, which accounts for the structural details of MTs and enjoys a greatly improved efficiency in studying MT mechanics relative to existing atomistic techniques. It is thus of timeliness to conduct an investigation on the influence exerted by the inter-*PF* sliding on the nanomechanics of MTs.

Motiviated by the idea the present study examined the effect of the inter-*PF* sliding on the static bending and transverse vibration of MTs. Here the 13-MTs consisting of 13 *PF*s are considered as a typical example. To estimate the effect of the inter-*PF* sliding the MSM technique was compared with the Euler beam model in calcualting the bending stiffness and the frequency of MTs.

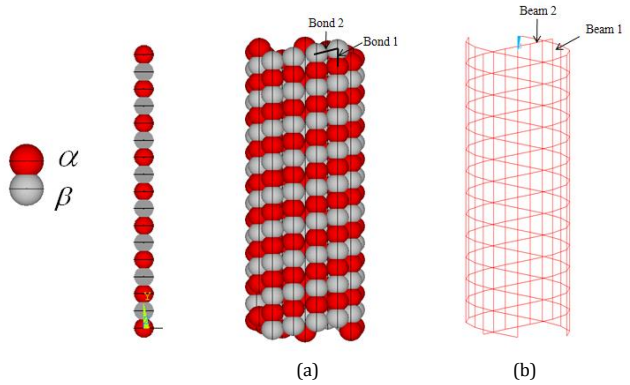

Fig. 1 (a) Illustration of α and β tubulins, a protofilament (*PF*) constructed by α and β tubulin and a microtubule comprising of laterally bonded *PF*s; (b) The equivalent frame structure of microtubules where beam 1 and beam 2 correspond to bond 1 (i.e., intra-*PF* $\alpha-\beta$ bonds) and bond 2 (i.e., inter-*PF* $\alpha-\alpha$ and $\beta-\beta$ bonds)

2. Experimental Methods

In the present study analyses will be carried out to calculate the bending stiffness and vibration frequency of MTs based on the MSM simulations and the equivalent continuum beam models.

2.1 Molecular Structure Mechanics Model

The force field of the molecular mechanics is expressed in the form of steric potential energy. They mainly include the bond stretching energy U_i^r, the angle bending energy $U_i^\emptyset$ and the dihedral angle torsional potential energyU_i^τ. The total potential energy U of an MT can be written as

$$U = \sum_{i=1,2}\left(\sum U_i^r + \sum U_i^\emptyset + \sum U_i^\tau\right) \quad (1)$$

The subscripts 1 and 2, respectively, denotes the longitudinal (i.e., intra-*PF* αβ interactions) and lateral (i.e., inter- *PF* αα or ββ interaction) directions (Fig. 1a). In the MSM, the intra-*PF* αβ bonds are modeled as elastic beam 1 and the inter- *PF* αα (ββ) bonds are treated as elastic beam 2. The sum of the potential energy of the frame structure shown in Fig. 1b is

$$U = \sum_{i=1,2}\left(\sum U_i^A + \sum U_i^M + \sum U_i^T\right) \quad (2)$$

*Corresponding Author
Email Address: *cywang@ujs.edu.cn (Chengyuan Wang)*

where U_i^A, $U_i^M$and U_i^T are the strain energies in a uniform beam due to tension, bending and torsion, respectively. The subscripts 1 and 2 denote the strain energies of the beam 1 and 2, respectively.

Such a frame structure is equivalent to an MT when the energies in Eq. 1 are equal to the corresponding energies in Eq. 2, which leads to

$$(YA)_i = k_i^r l_i, (YI)_i = k_i^{\emptyset} l_i, (SJ)_i = k_i^{\tau} l_i, \quad (i = 1,2) \tag{3}$$

where $(YA)_i$, $(YI)_i$and $(SJ)_i$are the extensional, bending and torsional stiffnesses of elastic beam i, respectively.k_i^r, $k_i^{\emptyset}$, and k_i^{τ} are the force constants for bond stretching/compression, bond angle bending, and bond torsion of MTs.In addition, l_i is the length of the equivalent beam i. The force constants of MTs are obtained from the coarse grain molecular dynamics simulation (CGMDS) performed in [12] where$(k_1^r)_{ref} = 3\ nN/nm$,$\left(k_1^{\emptyset}\right)_{ref} = 2\ nN/nmand(k_1^{\tau})_{ref} = 0.04\ nN/nm$were obtained for the intra-*PF* αβ bonds, and $(k_2^r)_{ref} = 14\ nN/nm$,$\left(k_2^{\emptyset}\right)_{ref} = 8.5\ nN/nm$, and $(k_2^{\tau})_{ref} = 0.17\ nN/nm$ were calculated for the inter-*PF* αα (ββ) bonds. Here subscript 'ref' means the value of the quantity obtained in [12]. The beam stiffness used in the present work can be calculated based on Eq. 3 and the above constants calculated in [12]. Subsequently, the nodal displacements can be obtained for the equivalent frame structures of MTs based on the stiffness matrix method. Readers may refer to [6-8] for more details of the MSM techniques.

2.2 Elastic Beam Models for MTs

In the Euler beam theory the dynamic equation for transverse vibration is as follows [17].

$$EI\frac{\partial^4 \omega}{\partial x^4} = \rho S\frac{\partial^2 \omega}{\partial t^2} \tag{4}$$

where ω is the transverse displacement of MTs, E is the Young modulus, I is the second moment of inertia, ρ is the mass density, S is the area of the cross section and t is time. The solution to Eq. 4 is in the form of $\omega(x,t) = W(x)e^{i\omega t}$ where $W(x)$ is the shape function, x is the coordinator in axial direction and ω is the angular frequency. Substitution of the solution into Eq. 4 gives the following equation.

$$EI\frac{d^4W(x)}{dx^4} - \rho S\omega^2 W(x) = 0 \tag{5}$$

The general solution to Eq. 5 is

$$W(x) = c_1 sin\alpha x + c_2 cos\alpha x + c_3 sh\alpha x + c_4 ch\alpha x \tag{6}$$

where c_1, c_2, c_3 and c_4 are coefficients to be determined by boundary conditions and $\alpha^2 = \omega\sqrt{\frac{\rho S}{EI}}$. Using Eq. 6 and the boundary conditions considered leads to a group of algebraic equations for c_1, c_2, c_3 and c_4. For nonzero solution of (c_1, c_2, c_3, c_4) associated with cantilever beams we have [17]

$$1 + \mu sin(\alpha l)sh(\alpha l) + cos(\alpha l)ch(\alpha l) = 0 \tag{7}$$

Solving Eq. 7 one can get α and then the frequency $f = \frac{\omega}{2\pi}$ via $\alpha^2 = \omega\sqrt{\frac{\rho S}{EI}}$ for cantilevered MTs.

3. Results and Discussion

In what follows, the MSM and the Euler beam theories will be employed to characterize the bending deformation and transverse vibration of 13-MTs whose lateral cylindrical surface comprises 13 *PF*s connected via the inter-*PF* $\alpha\alpha$ and $\beta\beta$ interactions. The attention will be focused on the influence of the inter-*PF* sliding on the bending stiffness and vibration frequency of MTs.

3.1 Static Bending of MTs

In this section the MSM technique was used to simulate the bending of the MT with one end clamped and the other free. As shown in Fig. 2a, in doing this we applied a concentrated force p to each of the 13 constituent *PF*s in transverse direction. Thus the MT was bent by a resultant force $13p$ acting on the free end of the cantilevered MT. First we would like to confirm that the MSM model is able to capture the inter-*PF* sliding which is considered as a result of the weak inter-*PF* bonds of MTs and observed experimentally in previous studies [3, 4]. To this end the MSM technique was used to perform bending experiment for the MT-like structures where the inter-*PF* bonds are very weak and characterized by the values of $(k_2^r)_{ref}$,$\left(k_2^{\emptyset}\right)_{ref}$, and $(k_2^{\tau})_{ref}$ four orders of magnitude smaller than those given by [12]. Indeed, as shown in Fig. 2b, the inter-*PF* sliding was clearly shown for the MT-like structure due to extremely weak inter-*PF* interaction. As a result the cross section originally normal to the neutral line (or the central line) is no longer perpendicular to it after the bending of the MT.

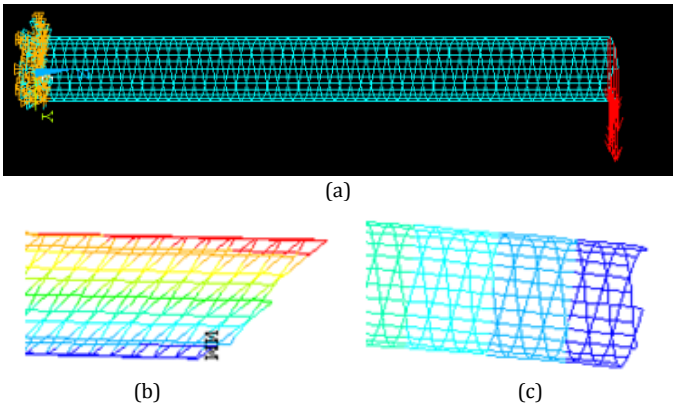

(a)

(b) (c)

Fig. 2 (a) Schematic for a cantilever MT subjected to a transverse resultant force P achieved by applying a force p on the free end of each *PF*, (b) the bending (with substantial inter-*PF* sliding) of the MT-like structure where the inter-*PF* interaction is four orders of magnitude weaker than that predicted by [12] for MTs, and (c) the beam-like bending (no inter-*PF* sliding) of MTs where the inter-*PF* interaction is predicted by [12] for MTs.

On the other hand, our simulations showed that when the relatively strong inter-*PF* bonds are considered, i.e., the values of $(k_2^r)_{ref}$,$\left(k_2^{\emptyset}\right)_{ref}$, and $(k_2^{\tau})_{ref}$ given by [12] are used, detectable inter-*PF* sliding cannot be easily observed for MTs. For example, the bending deformation is shown in Fig. 2c for the slender MT whose length-to-diameter ratio is 20. It is noted that the long MT seems to behave like an Euler beam where the cross section of the MTs remains a flat plane and perpendicular to the neutral line even after bending deformation. In other words, no significant inter-*PF* sliding would occur for the slender MTs. However, lack of direct observation does not necessarily mean that inter-*PF* sliding would not occur for MTs as the experimentally observed inter-*PF* displacement is only of the order of 0.1 nm [4] and thus difficult to observe directly in MSM simulations of the MTs whose diameter is around 25 nm and length is of the order of 100 nm. To solve this problem, an alternative method was proposed to detect the inter-*PF* sliding indirectly by examining its effect on the equivalent bending stiffness $(EI)_{eq}$ of MTs. The mechanism is that MTs without any inter-*PF* sliding will bend as Euler beams where the *PF*s above the neutral plane are stretched and those below the neutral plane are compressed. Specifically, a linear strain distribution will be established across the cross section of the MTs. This definitely will escalate tension in the structure and thus raise the bending stiffness of MTs. On the contrary, when the inter-*PF* sliding occurs the elongation and contraction of the *PF*s will be reduced. It therefore will ease the tension in the nanostructure and decrease the bending stiffness of the MTs.

In this method, the transverse deflection $f_{max}$of the free end was measured for the cantilevered MTs subjected to a transverse force $13p$. The obtained deflection $f_{max}$was then put into the formulae $(EI)_{eq} = \frac{PL^3}{3f_{max}}$ derived based on the Euler beam theory (without any inter-*PF* sliding) to evaluate the equivalent bending stiffness $(EI)_{eq}$ for 13-MTs. Here L represents the length of the MTs and $P = 13p$ is the transverse force acting on the free end. In this study while the diameter is fixed at around 25 nm the length-to-diameter ratio L/d considered for the MTs grows from 4.7 to 10, and 20. As shown in Table 1, in this process the equivalent bending stiffness $(EI)_{eq}$ is found to grow from $7.1 \times 10^{-24}\ Nm^2$, to $8.7 \times 10^{-24}\ Nm^2$ and $8.9 \times 10^{-24}\ Nm^2$. However, further raise the aspect ratio to 30 or even greater $(EI)_{eq}$ remains constant, i.e., $8.9 \times 10^{-24}\ Nm^2$, independent of length or L/d. The above length-dependence of $(EI)_{eq}$ achieved for relatively short MTs can be explained by the effect of the inter-*PF* sliding. In other words, the obtained value of $(EI)_{eq}$ reflects the effect of the inter-*PF* sliding on the bending of the MTs. Indeed, as shown in Fig. 3, longer MTs with a greater aspect ratio exhibit higher bending stiffness due to the smaller effect of the inter-*PF* sliding. In particular,

when the aspect ratio exceeds a critical value, e.g., 20, the length-dependence of $(EI)_{eq}$ disappears suggesting that no inter-*PF* sliding occurs for such slender MTs. In other words these long MTs behave like an Euler beam with a constant bending stiffness independent of the aspect ratio. To summarize, in this section the significant effect of the interlayer sliding is achieved for the bending of the MTs, which increases with decreasing length (or the half deformation wavelength) or the decreasing aspect ratio of MTs.

Table 1 Equivalent bending stiffness $(EI)_{eq}$ obtained for 13-MTs whose aspect ratio L/d increases from 4.7 to 50

Aspect ratio L/d	4.7	10.2	20	30	50
Bending stiffness $(EI)_{eq}$(10^{-24} Nm^2)	7.1	8.7	8.9	8.9	8.9

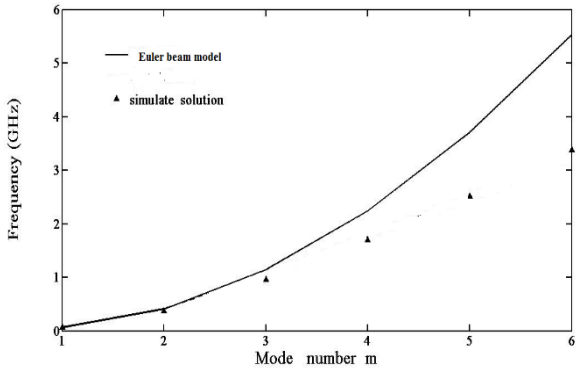

Fig. 3 Frequencies calculated for the first 6 modes (i.e., m = 1 to 6) of the transverse vibrations of 13-MT with the length-to-diameter ratio L/d = 10 based on MSM simulations (triangle dots) and the Euler beam mode (the solid line)

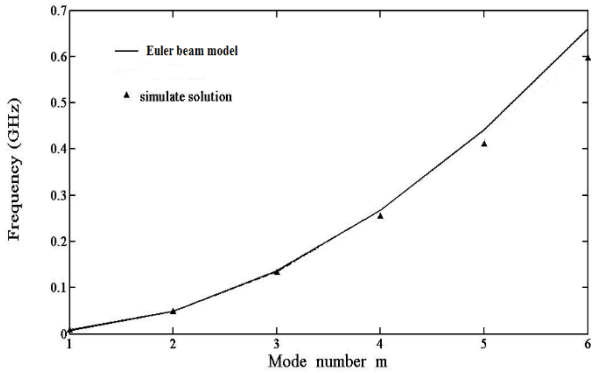

Fig. 4 Frequencies calculated for the first 6 modes (i.e., m = 1 to 6) of the transverse vibrations of 13-MT with the length-to-diameter ratio L/d = 30 based on MSM simulations (triangle dots) and the Euler beam mode (the solid line)

3.2 Transverse Vibration of MTs

In this section we further examined the effect of the inter-*PF* sliding on the transverse vibration of the cantilevered MTs, where bending deformation is predominant. The frequencies calculated based on the MSM able to account for the inter-*PF* sliding are compared with those given by the Euler beam model with the bending stiffness $(EI)_{eq} = 8.9 \times 10^{-24}\ Nm^2$, i.e., the effect of the inter-*PF* sliding is not considered in this model. The effect of the inter-*PF* sliding on the vibration of the MTs can then be measured by comparing the MSM techniques with the Euler beam model in predicting the frequency of the MTs.

Here the frequencies of modes 1 to 6 obtained based on the MSM technique (i.e., f_{msm} represented by the triangle dots) were plotted in Figs.3 and 4 for MTs with the aspect ratio L/D = 10 and 30, respectively. For sake of comparison the corresponding results computed by using the Euler beam model (i.e., f_{beam} represented by the solid line) are also shown in the two figures. It is noted in Fig.3 that difference between the two techniques is small and not easy to observe when models 1 and 2 are considered. It however grows with the rising mode number m and becomes substantial at m = 4, 5 and 6 with the relative difference defined by $\frac{f_{beam}-f_{msm}}{f_{msm}} \times 100\%$ rising from 37% to 48% and to 63%. In addition, it is noticed that while m increases from 1 to 6 the corresponding half wavelength-to-diameter ratio $L/(md)$ decreases from 10 to 1.7. Thus the above results indicate that the beam model will substantially overestimate the frequency for the high transverse vibration modes of MTs with relatively short half wavelength (e.g., $L/(md)$ is small) as it is unable to account for the effect of the inter-*PF* sliding. It thus follows that the effect of the inter-*PF* sliding is more substantial for higher vibration modes of the MTs with smaller axial half wavelength. This result is found to be consistent with the conclusion drawn in the prior section for the bending of the 13-MTs.

In Fig. 4 for longer MTs with $\frac{L}{d} = 30$ very similar trend is observed for the dependence of the effect of the inter-*PF* sliding on the half wavelength-to-diameter ratio $L/(md)$. However the relative difference $\frac{f_{beam}-f_{msm}}{f_{msm}} \times 100\%$ between the MSM and the Euler beam model ranges from 8% to 11% for vibration modes 4 to 6, much smaller than the corresponding values obtained above for the relatively short MTs with $\frac{L}{d} = 10$. This observation is not surprising as L/d considered in Fig. 4 is three times of L/d selected in Fig. 3. Accordingly, for the same mode number m the half wavelength-to-diameter ratio $L/(md)$ or the wave length in Fig. 4 is always three times as much as the one considered in Fig. 3. It is clearly seen from the above results that the effect of the inter-*PF* sliding turns out to be smaller for the vibration of the slender MTs with a greater half wavelength or the half wavelength-to-diameter ratio. In addition, the comparison of the results, the inter-*PF* sliding may exert more significant influence on the high mode frequency than it does on the bending stiffness of the MTs. This is simply because that the high mode vibration may have very short wavelength even if the length of the MTs is relatively large.

The length dependence of the inter-*PF* sliding effect can be attributed to the fact that the sliding is controlled by the individual inter-*PF* bonds whose number increases with the length of the MTs or the wavelength of the vibration. Thus to achieve the same inter-*PF* displacement energy barrier need to be overcome would be smaller for bending or vibration of MTs with a smaller length. In other words the effect of inter-*PF* sliding becomes greater for the deformation of MTs with a shorter axial wavelength.

It is worth mentioning here that the results obtained in the present study are based on the force field coefficients given by the molecular dynamics simulations [12]. However large discrepancy is found among different studies in evaluating the coefficients for the inter-*PF* bonds. In particular, in some previous work much weaker inter-*PF* interaction is reported for MTs. If this is the case the above-mentioned effect of inter-*PF* sliding can be much more pronounced than what was reported in this study.

4. Conclusion

The MSM technique enables one to exam the effect of the inter-*PF* sliding on the mechanics of the MTs. This method thus was employed to study the static bending and the transverse vibration of 13-MTs. The effect of the inter-*PF* sliding was then revealed by comparing the MSM simulations with the corresponding results given by the Euler beam theory where the inter-*PF* sliding is completely excluded. The new findings are summarized as follows.

It is found that the inter-*PF* sliding occurs for the MTs due to the weak interaction between adjacent *PF*s. The occurrence of the inter-*PF* sliding will ease the tension in MTs generated by the bending deformation and thus results in lower bending stiffness of MTs. This effect is significant for MTs with small aspect ratio, e.g., $L/d < 10$. It then decreases with rising L/d and becomes negligible for MTs with $L/d \geq 30$, i.e., no inter-*PF* sliding occurs for relatively long MTs. Thus, the inter-*PF* sliding leads to the size-dependent equivalent bending stiffness of relatively short MTs whose aspect ratio is smaller than 30.

Accordingly inter-*PF* sliding also significantly down shifts the frequency of transverse vibration of MTs relative to the frequency given by the Euler beam with the same axial extensional stiffness and geometric size. In particular such an effect is more substantial for higher vibration mode of MTs with small half wavelength-to-diameter ratio. Thus the effect of the inter-*PF* sliding can still be significant for the high modes of the slender MT with $L/d \geq 30$.

References

[1] J. Howard, Mechanics of motor proteins and the cytoskeleton, Sinaure Associates Publishers, USA, 2001.
[2] J. Howard, A.A. Hyman, Dynamics and mechanics of the microtubule plus end, Nature 422 (2003) 753-758.
[3] D. Chretien, H. Flyvbjerg, S.D. Fuller, Limited flexibility of the inter-protofilament bonds in microtubules assembled during from pure tubulin, J. Eur. Biophys. 27 (1998) 490-500.
[4] D. Chretien, S.D. Fuller, Microtubules switch occasionally into unfavorable configuration during elongation, J. Mol. Biol. 298 (2000) 663-676.

[5] A. Kis, S. Kasas, B. Babić, A.J.Kulik, W. Benoît, G.A.D. Briggs, Nanomechanics of microtubules, Phys. Rev. Lett. 89 (2002) 248101.
[6] C.Y. Wang, C.Q. Ru, A. Mioduchowski, Vibration of microtubules as orthotropic elastic shells, Physic. E 35 (2006) 48-56.
[7] C.Y. Wang, C.Q. Ru, A. Mioduchowski, Orthotropic elastic shell model for buckling of microtubules, Phys. Rev. E 74 (2006) 052901-ENDPAGE.
[8] C.Y. Wang, L.C. Zhang, Circumferential vibration of microtubules with long axial wavelength, J. Biomech. 41 (2008) 1892-1896.
[9] F. Pampaloni, E.T. Florin, Microtubule architecture: Inspiration for novel carbon nanotube-based biomimetic materials, Trends Biol. 26 (2008) 302-310.
[10] T.Li, A mechanics model of microtubule buckling in living cells, Biomech. 41 (2008) 1722-1729.
[11] C.Y. Wang, C.F. Li, S. Adhikari, Dynamic behaviors of microtubules in cytosol, J. Biomech. 42 (2009) 1270-1274.
[12] X.Y. Ji, X.Q. Feng, Coarse-grained mechanochemical model for simulating the dynamic behavior of microtubules, Phys. Rev. E. 84 (2011) 4146-4152.
[13] X. Ping, K.M. Liew, Predicting buckling behavior of microtubules based on an atomistic-continuum model, Int. J. Solids Struc. 48 (2011) 1730-1737.
[14] J. Zhang, S.A. Meguid, Buckling of microtubules: An insight by molecular and continuum mechanics, Appl. Phys. Lett. 105 (2014) 173704.
[15] J. Zhang, C.Y. Wang, Molecular structural mechanics model for the mechanical properties of microtubules, Biomech. Model Mechanobiol. 13 (2014) 1175-1184.
[16] J. Zhang, C.Y. Wang, Free vibration analysis of microtubules based on the molecular mechanics and continuum beam theory, Biomech. Model Mechanobiol. (2015) (In Print).
[17] J.N. Reddy, S.D. Pang, Nonlocal continuum theories of beams for the analysis of carbon nanotubes, J. Appl. Phys. 103 (2008) 023511.

Cite this Article as: Zhigang Guo, Chengyuan Wang, The effect of inter-protofilament sliding on the mechanics of microtubules, J. Nanosci. Tech. 2(2) (2016) 122–125.